Development of a Hybrid Fast Ion Transport Code with Bounce Time-Step-Based Orbit-Following and Drift Orbit-Following

Kouji SHINOHARA[1,3)]*, Keiji TANI[2)], Nobuhiko HAYASHI[3)], Shuhei SUMIDA[3)], Akira EJIRI[1)], Naoto TSUJII[1)], Takeru INOUE[1)], Masanobu SUZUKI[3)], Andreas BIERWAGE[3)], Yu-Ting LIN[1)], Yiming TIAN[1)], Fumiya ADACHI[1)], Shunya ABE[1)], Yuta TAKECHI[1)]

[1)] *The University of Tokyo, Chiba 277-8561, Japan*
[2)] *Kyoto Fusioneering, Tokyo 100-0004, Japan*
[3)] *QST, Naka Institute for Fusion Science and Technology, Ibaraki 311-0193, Japan*

(Received 16 September 2025 / Accepted 23 October 2025)

We developed a bounce-time-based (BT) orbit-following Monte-Carlo code in order to calculate a fast ion transport in the previous work as an extension of the OFMC code in QST. In the BT method, we take a bounce time as a time step of the orbit following for the purpose of reducing computational resources. However, the BT method code has limitations in its realistic application. In order to reduce the limitation, we have developed a hybrid code with the BT method and a drift orbit-following method. In the code, we can switch the methods depending on conditions for each purpose. With using this hybrid code, we have reduced the difference between the BT method and drift orbit-following method in the distribution of fast ions and heating in the plasma central region, which was observed in the previous work, and have been able to adopt a realistic first wall as a loss boundary instead of a separatrix. We have also applied this hybrid approach to handle a fast ion transport in a toroidal field ripple. The hybrid calculation well reproduced the profiles of several quantities obtained by the drift orbit calculation alone while reducing the calculation time.

Keywords: fast ion transport, bounce time, finite orbit width, Monte Carlo code, tokamak

DOI: 10.1585/pfr.20.1403058

1. Introduction

When designing power reactors or DEMO reactors, calculation codes are required to develop and optimize operation scenarios which are consistent with heating system, confinement, heat handling in the divertor. Such codes are being developed as integrated codes. In Japan, the development of TOPICS [1] and TASK [2, 3] is active.

An important element in developing plasma operation scenarios is the evaluation of heating, current, and momentum drive of bulk plasma. Important drive sources are alpha particles from fusion products and fast ions coming from neutral particle beams. In the integrated code TOPICS in QST, OFMC [4] is responsible for evaluating the heating, current, and momentum drive caused by these fast ions.

The evaluation of heating, current, and momentum drive by fast ions is not limited to the reactor design, but is also required for analyzing experimental results, and is required in advance to achieve desirable heating and current profiles for efficient experiments. The OFMC code has contributed to the analysis of experiments in JT-60U [5, 6], JFT-2M [7], JET, DIII-D [8], and has also contributed to the development of operational scenarios for JT-60SA [9] and ITER [10–13].

It is required that such evaluations be carried out in realistic conditions such as a fast ion source distribution, plasma configuration, and loss boundary. To address this requirement, Monte-Carlo-based method has been used, in which the full-orbit or drift-orbit trajectories of a large number of test particles are followed. The OFMC code adopts this method. A drawback of this method is the need for a large number of test particles to improve the accuracy of the distribution, which is determined by Monte-Carlo noise, and another drawback is that a large computational resource is required as a result. This is a bottleneck for an efficient analysis and operational scenario design, which requires parameter scans. Therefore, we introduced a new orbit-following method in 3D phase space using the bounce period, τ_B, as a time step into the OFMC. Using the bounce period as the time base is similarly applied when solving the Fokker-Planck equation by using the bounce-time averaged quantities. We applied this bounce-time-based (BT) method to the OFMC code, and achieved a speedup of approximately 70 times (or reduced computational

*Corresponding author's e-mail: shinohara@k.u-tokyo.ac.jp

resources) in the JT-60U case in the previous work [14].

However, in the previous paper, there were some differences between the BT and drift-orbit-following (or guiding-center-following; GC) methods in the distribution of fast ions and heating in the plasma central region. In addition, the loss boundary of fast ions was a plasma surface or a separatrix, namely particle loss was not properly handled. Such issues should be resolved.

Since we implemented the BT method in the OFMC which can utilize the GC method, we can easily achieve a hybrid approach of the BT method and the GC method. In the hybrid approach, while the BT method is the basis, particles that meet certain conditions are followed using the GC method. We have resolved the above issues in the previous work by the hybrid approach. In addition, we have also attempted a calculation for a fast ion transport in a toroidal magnetic field (TF) ripple by the approach.

In this paper, we briefly review the BT method and describe the abstract of the workflow of the hybrid code in Sec. 2. We report the reduction of the differences in the profiles observed in previous work by using the GC method for shallowly trapped particles in Sec. 3. We describe the application of the hybrid code to handle a realistic loss boundary or an axisymmetric first wall in Sec. 4. In Sec. 5, we applied this hybrid approach to handle the fast ion transport in a TF ripple. Finally, a summary and future plans are described in Sec. 6.

2. Review of BT Method and Abstract of Workflow of Hybrid Code

Here, we review the BT method. In an axisymmetric tokamak configuration, three quantities—canonical toroidal angular momentum P_φ, energy E, and pitch parameter Λ are conserved without a collision. If the collision time is sufficiently longer than the bounce time, the trajectory projected onto a poloidal plane from a trajectory in a 3D real space can be determined by these quantities. These three quantities (P_φ, E, Λ) are conserved as long as there is no collision. Conversely, these quantities (P_φ, E, Λ) change with a collision. The sequential changes correspond to a test particle moving through 3D phase space or the 3D phase-space transport of the test particle. In the BT method, the bounce time, τ_B, is used as the collision interval. The calculation of the 3D phase-space transport of test particles results in the phase-space distribution of fast ions. Furthermore, we obtain the heating and momentum-drive distribution of the bulk plasma by evaluating the energy and momentum exchanges due to the collisions with the bulk plasma. We employ the Trubnikov model [15], as in the conventional OFMC or in the GC method, for collisions with the bulk plasma to accommodate discretization of the collision interval.

Due to a magnetic drift, a particle orbit deviates from a poloidal flux surface (the finite orbit width effect). Collisions, i.e. interactions, between a test particle which is a fast ion, and bulk particles are determined by parameters on the orbit. Therefore, to evaluate collisions with bulk plasma, the information on the relationship between a point on the orbit and a poloidal flux surface is required since parameters connected with the bulk plasma are expressed as functions of the poloidal flux. In other words, a real-space particle orbit is required. In the conventional OFMC, the real-space orbit is directly obtained using an orbit calculation based on Newton's equation of motion, or a calculation based on the drift equation (referred to as the GC method in this paper). In the BT method, however, we take advantage of the fact that a particle orbit in real space can be well approximated as shown below. Assuming axisymmetry, $B_\varphi \sim B$, and that the toroidal field strength is inversely proportional to the R or $C_B \equiv B_\varphi R$ = const. (i.e., ignoring the diamagnetic effect), we obtain

$$\psi_p = \hat{P}_\varphi + \mathrm{sign}(v_\parallel)\frac{\sqrt{2EM}}{q}\sqrt{R(R-R_{TIP})}, \tag{1}$$

from the definition of the canonical toroidal angular momentum P_φ, energy E and pitch parameter Λ. Here, ψ_p is the poloidal flux function,

$$\hat{P}_\varphi \equiv P_\varphi/q, \tag{2}$$

(this form $\hat{P}_\varphi$ is also known as ψ_p^*), $\mathrm{sign}(v_\parallel)$ is the sign of the velocity of the particle against the plasma current, the q the electric charge of the particle, the M the mass of the particle, the R the major radius and

$$R_{TIP} \equiv \frac{\mu C_B}{E}. \tag{3}$$

When we specify a radial position R, the right-hand-side of the Eq. (1) is determined for a given set of (P_φ, E, Λ, $\mathrm{sign}(v_\parallel)$), then we can specify a poloidal flux. Equation (1) describes the relation between R and ψ_p. Then, we can determine two vertical positions using a mapping of $\psi_p \leftrightarrow (R, Z)$ since a specific poloidal flux passes two vertical positions at a specific radial position inside a separatrix. In this way, we can have the poloidal projection of an orbit for a given set of (P_φ, E, Λ, $\mathrm{sign}(v_\parallel)$) from this Eq. (1). For a passing particle, its R is taken between the minimum value R_h and maximum value R_l on its orbit as shown in Fig. 1. For a trapped particle, its R is taken in $R_{TIP} < R < R_{CTR}$ and $R_{TIP} < R < R_{CO}$, where R_{CO}, R_{CTR}, and R_{TIP} are shown in Fig. 1. Note that we take $\psi_p = 0$ on the separatrix and $\psi_p < 0$ in the main plasma region.

In this study, we have carried out a hybridization of the GC method and the BT method. The GC method or the BT method in the OFMC code works according to the flow shown in Fig. 2. Both methods track test particles. The test particles are generated and used based on the Monte-Carlo method. The hybridization can be achieved by controlling whether the test particles follow the GC method or the BT method. We consider a specific case where a loss boundary is a first wall in order to explain the specific flow of the hybrid calculation (Fig. 3). First, the possible values of ψ_p on an orbit are calculated using Eq. (1). If a value takes $\psi_p \geq 0$, then the test particle is considered to be a loss particle in the case of the BT method alone. However, in the case of the hybrid code, the

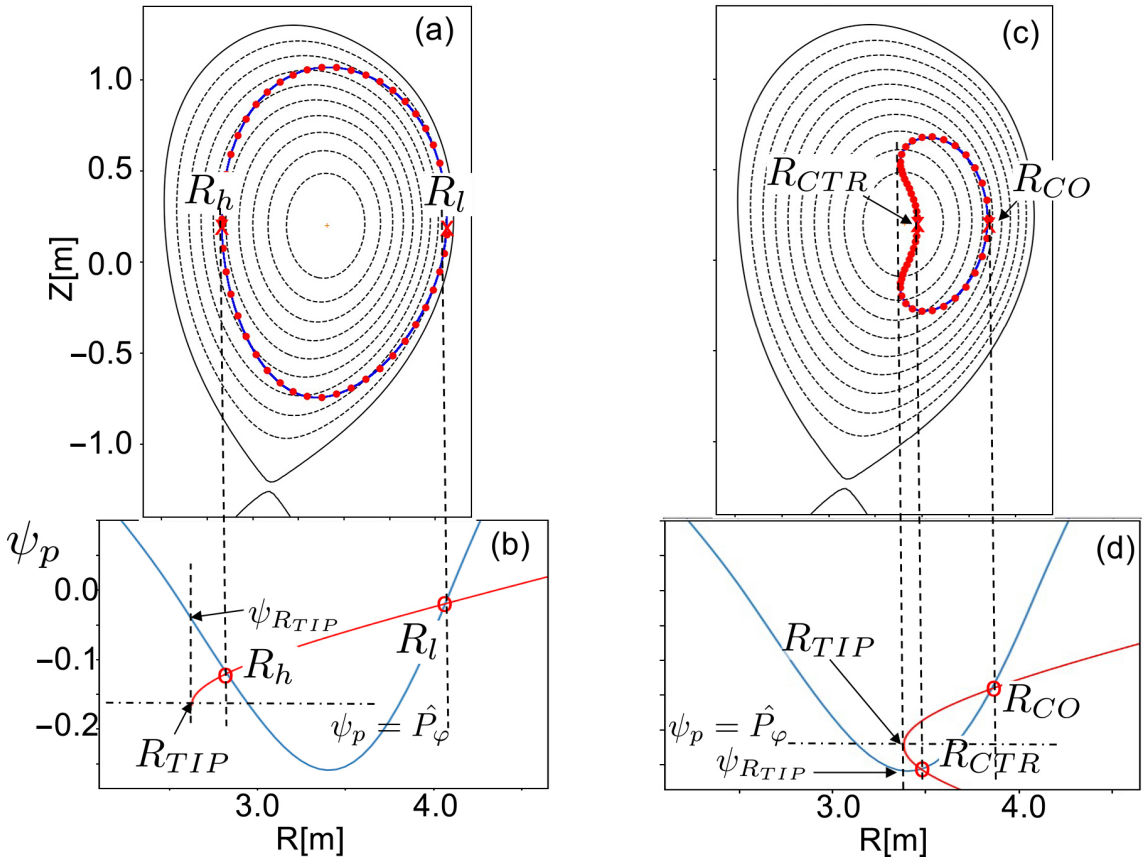

Fig. 1. Poloidal projection of an orbit for a co-passing particle (a), and for a banana (trapped) particle (c). The particle species is deuteron. The points obtained by Eq. (1) are shown in red closed circles. The blue curve represents the orbit obtained by the GC calculation. The R_h, and R_l are the major radius values of the passing orbit on the midplane on the higher and lower field side, respectively. The R_{CTR}, and R_{CO} are the major radius values of the banana orbit on the midplane on the higher and lower field side, respectively. The R_{TIP} is the major radius value defined by Eq. (3). In the (b) and (d), the red curves represent Eq. (1), and the blue curves are the poloidal flux function on the mid plane. The major radiuses of the intersections of these curves give the R_h, R_l, R_{CTR}, and R_{CO}, respectively. The horizontal dashed-dot line represents $\psi_p = \hat{P}_\varphi$. The $\psi_{R_{TIP}}$ is the value of the poloidal flux function on the midplane at $R = R_{TIP}$.

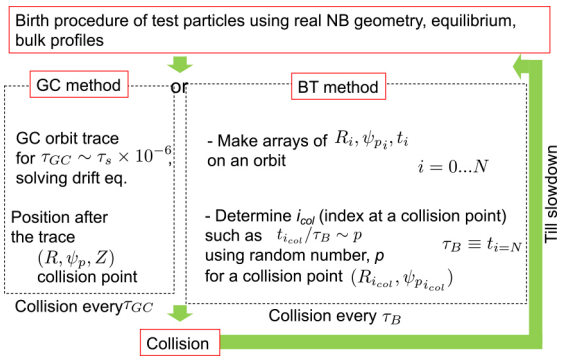

Fig. 2. Calculation flow in OFMC for the GC method or BT method.

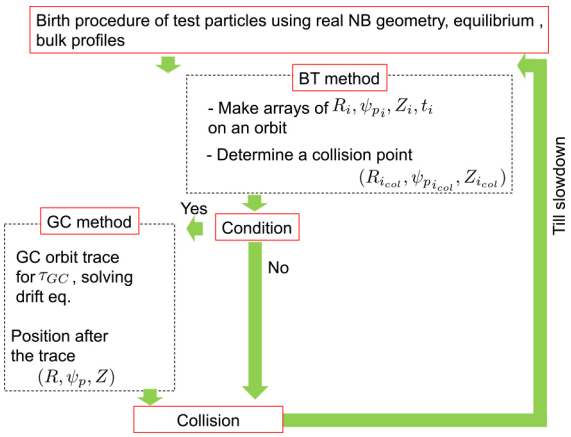

Fig. 3. Calculation flow in OFMC for the hybrid calculation.

calculation of such an orbit is switched to the GC method. The starting position (R, Z) of the GC calculation is selected by taking into account the time coordinate normalized by the bounce time, τ_B. The selection is the same with the selection of a collision point [14]. The normalized time coordinate takes 0 to 1. Then, the point (R, Z) where the normalized time coordinate is equal to a uniform random number generated between 0 and 1 is selected (see also Fig. 2).

The GC method calculates a trajectory for τ_{GC} ($\sim \tau_s \times 10^{-6}$ which is the standard value for the GC calculation in the OFMC, based on results in past runs) and performs a collision procedure. As the result of the collision, parameters (P_φ, E, Λ, sign($v_\parallel$)) change. If the values of ψ_p obtained by Eq. (1) for the new parameters always get $\psi_p < 0$, the particle is followed by the BT method. If a value can still take $\psi_p \geq 0$, then we keep using the GC method. As can be seen from Fig. 3,

the hybrid code evaluates the condition whether $\psi_p \geq 0$ or not via the BT method (or Eq. (1)). This performing of the BT method involves an overhead. However, since the computational load of the BT method is small, if the GC method is used less frequently, we can expect a faster calculation by the hybrid code than by the GC method alone.

In this example of a realistic loss boundary, the condition for switching between the GC method and the BT method is whether $\psi_p \geq 0$ or $\psi_p < 0$. By changing this condition, it becomes possible to handle various applications.

In the following sections, we will show examples of hybrid calculations. The plasma equilibrium (Bt / Ip = 1.2 T / 0.6 MA) is shown in Fig. 1, and the conditions for the electron density distribution, electron and ion temperature distribution, and injected neutral particle beam (NB) are the same as those in the previous paper [14]. All injected NBs are those from positive ion sources with a maximum beam energy of 85 keV, and the power is 2 MW for the co-injection or for the injection in the direction to the plasma current, 2 MW for the counter-injection, and 2 MW for the perpendicular injection. The number of test particles is 20,000.

Section 3 shows the case when the condition is for shallowly trapped particles, Sec. 4 shows the case when the condition is for a realistic loss boundary, and Sec. 5 shows the case to handle a fast ion transport in a TF ripple in this hybrid code.

3. Condition for Shallowly Trapped Particles

In the previous paper, there were some differences between the BT and GC methods in the distribution of fast ion energy density and heating around the magnetic axis. The difference in the distribution is thought to be due to shallowly trapped particles with inner legs near the magnetic axis [14]. Here, the inner leg indicates the part of a trapped (banana) orbit which lies on the side of the magnetic axis or has its major radius between R_{TIP} and R_{CTR}.

Therefore, we implemented the condition so that trapped particles that meet the following condition are tracked by the GC method. The condition for the GC method is that the value ψ_{pN} of the banana tip is less than 0.2 and that the ψ_{pN} of R_{CTR} is less than 0.05. Here, ψ_{pN} is the poloidal flux function normalized by the poloidal flux function value on the magnetic axis, $\psi_{pN} \equiv 1 - \psi_p/\psi_{p,AXIS}$. We call this condition Condition 1 in this paper.

The results are shown in Fig. 4. The results are for Condition 1 (solid curves), the GC method alone (dotted curves), and the BT method alone (dashed-dot curves). Note how to obtain these quantities is described in Ref. 14. The horizontal axis is the ψ_{pN}. The differences in distribution are mitigated. The computation time was ~ 1/30 to the GC method, compared to ~ 1/70 for the BT method alone in this case.

To shorten the calculation time, it is desirable to minimize the number of cases where the transition to the GC method is required. We assume that the longer the particle stays in the part of interest in the inner leg, the larger the contribution.

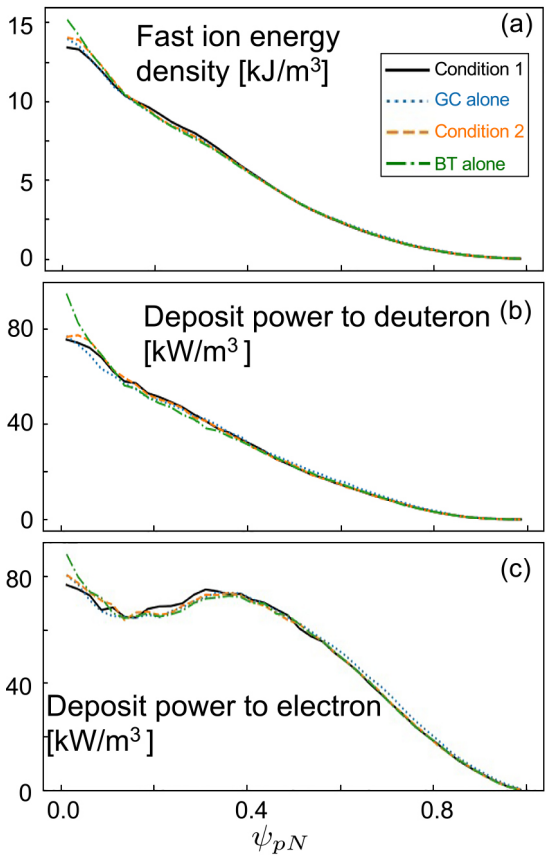

Fig. 4. Comparison of profiles of fast ion energy density (a), deposit power to bulk deuterons (b), and deposit power to bulk electrons (c). The results are depicted by black solid curves for Condition 1, blue dotted curves for the GC method alone, orange dash curves for Condition 2, and green dashed-dot curves for the BT method alone.

Then, the particle with relatively small velocity would contribute to this mechanism. We apply the Condition 1 to particles with relatively small velocity or low energy. On the other hand, since the orbit width effect is smaller for particles with lower energy, it is expected that too low energy value will be meaningless. Therefore, a scan of the reference energy was carried out. As a result, it was found that particles with an energy of less than 40 keV showed sufficiently good results (dash curves in Fig. 4). We call this Condition 2. In this case, the calculation time was ~ 1/40 to the GC method.

This value of 40 keV is comparable to the critical energy at which the energy transfer from fast ions to bulk ions and the transfer to electrons are comparable. Particles with its energy lower than the critical energy experience a larger pitch angle scattering at a collision. This might suggest the pitch angle scattering plays a role on the population of such shallowly trapped particles near the banana-passing boundary.

4. Condition for Realistic Loss Boundary

In reality, the boundary where fast ions are lost is a first wall. However, in the BT method alone, the loss boundary was a plasma surface or a separatrix to make the condition

simple. The condition for the loss determination in the BT method alone is whether $\psi_p \geq 0$ or not by evaluating Eq. (1).

The conventional OFMC which uses the GC method can determine collisions between particles and a first wall with an arbitrary shape. Therefore, by applying the GC method to the particle orbit that crosses the separatrix, it is possible to treat a first wall as the loss boundary. We treat the first wall as an axisymmetric shape since the BT method assumes an axisymmetric system and does not hold the positional information in the toroidal direction.

The results of this hybrid calculation with a first wall as the loss boundary are shown in Figs. 5–7. The Condition 2 described in Sec. 3 was also applied in this hybrid calculation. In Fig. 5, the particle loss locations are shown using dots. We can see a good agreement in the divertor region and on the baffle plate. The number density of the loss particles is high around the divertor strike points though the feature is hard to see in the figure. This feature appears in the both cases. The profiles for several quantities are compared in Figs. 6 and 7 for the hybrid calculation (solid curves) and the results using the GC method alone (dotted curves). We can see good agreements. The dashed curves indicate the case by the GC method alone in which the loss boundary is the separatrix. When the first wall is the loss boundary, we can see an increase in the fast ion energy density and heating in the plasma edge region, as well as the increase in the current drive and momentum drive, compared with the case when the separatrix is the loss boundary. Table 1 shows the total energy transfer ratio, total loss amount ratio, contribution ratio of thermalized test particles to the input power, and the calculation time for these three cases. The calculation time for the hybrid calculation was approximately 1/20, compared with the calculation by the GC method alone.

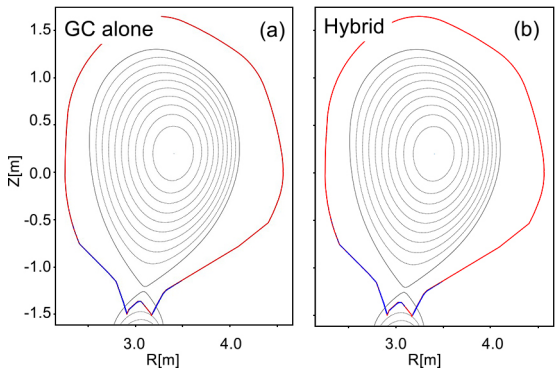

Fig. 5. Particle loss locations on the wall shown by using blue dots. (a) is the result for the calculation by the GC method alone, and (b) for the hybrid calculation.

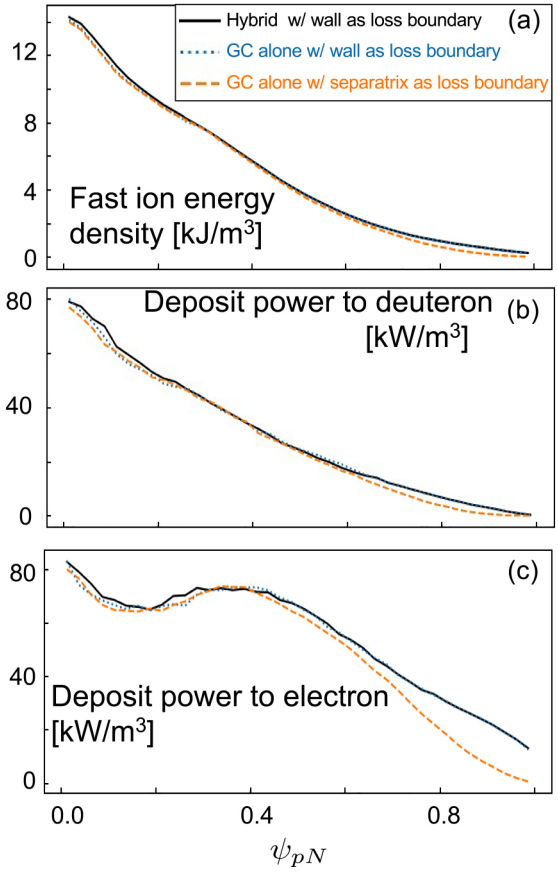

Fig. 6. Comparison of profiles of fast ion energy density (a), deposit power to bulk deuterons (b), and deposit power to bulk electrons (c). The results are depicted by black solid curves for the hybrid calculation with the first wall as the loss boundary, blue dotted curves for the calculation by the GC method alone with the first wall as the loss boundary, and orange dashed curves for the calculation by the GC method alone with the separatrix as the loss boundary.

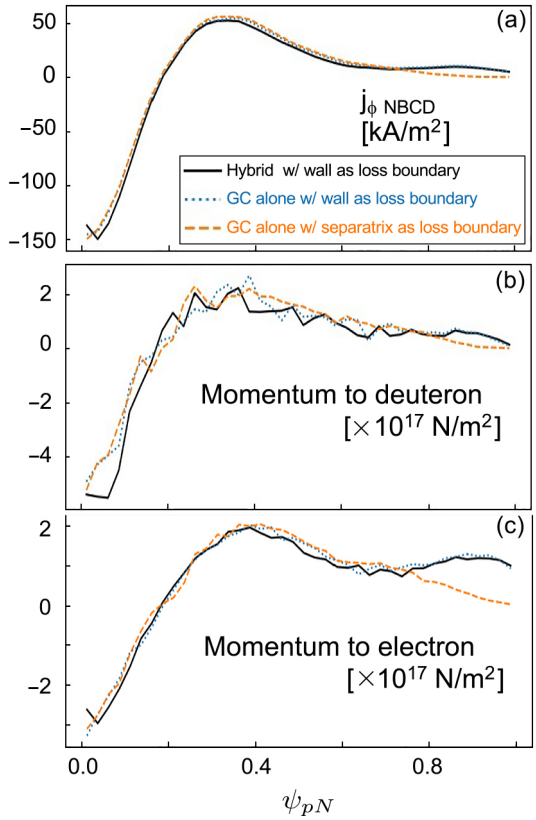

Fig. 7. Comparison of profiles of driven-toroidal-current density (a), momentum to bulk deuterons (b), and momentum to bulk electrons (c). The line-types are the same with those in Fig. 6.

Table 1. Total energy transfer ratio, total loss amount ratio, contribution ratio of thermalized test particles to input power, and calculation time.

	GC alone w/ wall as loss boundary	Hybrid w/ wall as loss boundary	GC alone w/ separatrix as loss boundary
Energy to Electron	55.7%	56.1%	49.0%
Energy to Ion	26.8%	27.0%	25.6%
Energy to Impurity	8.0%	7.6%	7.6%
Loss	8.2%	7.6%	16.6%
Contribution of thermalized test particles	1.3%	1.7%	1.2%
Calculation time [minutes]	85.4	4.2	79.9

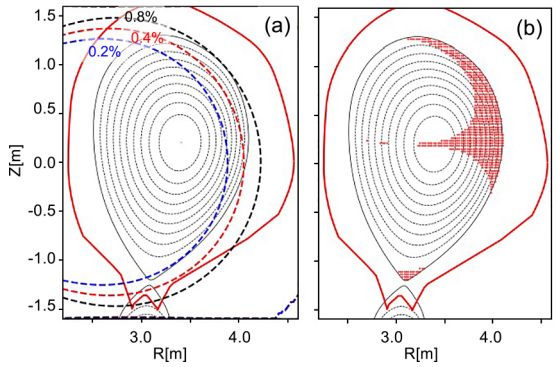

Fig. 8. Amplitude distribution of the TF ripple (a) and the ripple well region (b) on a poloidal cross section.

The condition that the separatrix is the loss boundary not only leads to an overestimation of losses but also affects the distribution.

The difference in the result suggests the importance of the effect of the finite orbit width. Due to the finite orbit width, a particle can go in and out the bulk plasma. Thus, the wall position affects the heating distribution. The distribution of various physics quantities especially in the plasma edge cannot be properly evaluated without considering the finite orbit width effect.

This result also indicates the profiles in the edge region are affected by the clearance between the separatrix and the wall.

These suggest the importance of a high plasma current in high-β plasma. With a higher plasma current, the orbit width effect becomes smaller, allowing the distance between the wall and the separatrix to be made narrower without a loss. This narrow clearance is particularly important for high-β plasmas, which require a wall stabilization.

5. Condition to Handle Fast Ion Transport in a Toroidal Field Ripple

The amplitude distribution of the TF ripple before the installation of ferrite steel tiles in JT-60U [6] is shown in Fig. 8(a). The ripple amplitude of larger than 0.2% is observed in the $\psi_{pN} > 0.4$. The ripple well for this configuration is also shown in Fig. 8(b).

It can be seen from Eq. (1) that the toroidal canonical angular momentum of the banana particle divided by the charge, $\hat{P}_\varphi$, is the poloidal flux function of the banana tip

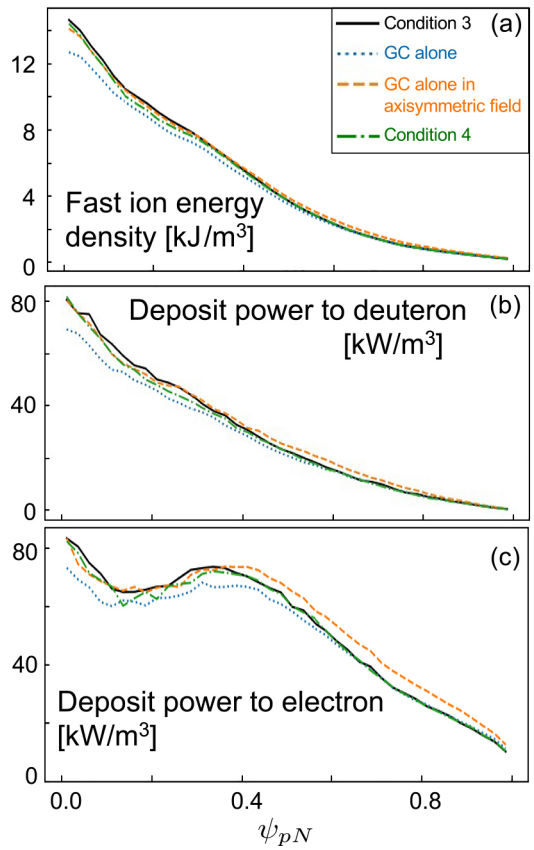

Fig. 9. Comparison of profiles of fast ion energy density (a), deposit power to bulk deuterons (b), and deposit power to bulk electrons (c). The results are depicted by black solid curves for Condition 3, green dashed-dot curves for Condition 4, blue dotted curves for the GC method alone in the TF ripple and orange dashed curves for the GC method alone in the axisymmetric field.

position of a banana particle, $\psi_{p,TIP}$. Since the resonant transport of banana tips seems to be a dominant mechanism for the fast ion transport by the TF ripple when collisions are less frequent, we set the condition (this is called Condition 3) that the banana tip is on the low-field side (i.e., the major radius of the banana tip, R_{TIP}, is larger than the major radius of the magnetic axis, R_{AXIS}), and $\psi_{pN,TIP} > 0.4$ as the first step. We set the loss boundary at the first wall. Figure 9 shows a comparison. We show the results for the Condition 3 with the solid curves, the GC method alone with the dotted curves, the case by the GC method alone in Sec. 4 or in the axisymmetric case with the dashed curves (in the following Figs. 12–15,

for a comparison, the results of the calculation by the GC method alone are always plotted with dotted curves, and the results of the calculation by the GC method alone in the axisymmetric field in Sec. 4 are also always plotted with the dashed curves). As shown in Figs. 9(b) and (c), the heating distribution is close to the dotted curves or the result of the calculation by the GC method alone at the periphery, but a difference can be seen in the $\psi_{pN} < 0.4$.

In the TF ripple transport, a collision effect near the banana tip is also important, but the collision position of the BT method is determined by random numbers based on a transit or staying time on an orbit. For this reason, it seems that the longer the collision interval, the relatively fewer opportunities for a collision near banana tips. To avoid the longer interval for a collision, we set an upper limit to the interval in addition to the Condition 3. This is called Condition 4. Since the interval is the bounce time, τ_B, in the BT method, we switch to the GC method when τ_B is longer than the upper limit. The upper limit of $2 \times 10^{-4} \times \tau_s$ was selected after a scan of the value so that the result is close to that by the GC method alone and so that the calculation time is not long. The result of this Condition 4 is shown in dashed-dot curves in Fig. 9. We can see a slight improvement from the Condition 3 alone.

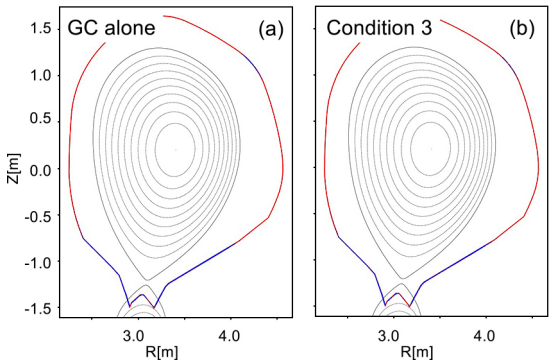

Fig. 10. Particle loss locations on the wall shown by using blue dots. (a) is the result for the GC method alone in the TF ripple field, and (b) for Condition 3.

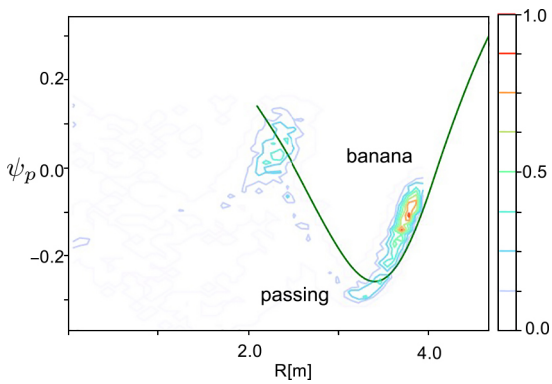

Fig. 11. Distribution of the (R_{TIP}, $\hat{P}_\varphi$) of lost particles at their birth time for the calculation by the GC method alone. The solid curve is the boundary between banana and passing orbits. The upper region of the curve is for banana orbits and vice versa.

The loss distribution to the wall is shown in Fig. 10 for the GC method alone and the Condition 3. We can see the loss in the upper part on the low-field-side as well as the divertor region and on the baffle plate. The distribution of the loss shows a good agreement, indicating that the hybridization is working properly.

Figure 11 shows the distribution of the R_{TIP}, defined by Eq. (3), and $\hat{P}_\varphi$ of the lost particles at their birth time for the calculation by the GC method alone. We found that some particles were near the solid curve, which is the boundary between banana (trapped) and passing (untrapped) particle orbits. This suggests that the contribution of passing particles changing into banana particles due to collisions is important. Therefore, we decided to track particles near the boundary between banana and passing particle orbits by using the GC method. The condition (Condition 5) was set in a way when the absolute difference between the $\psi_{R_{TIP}}$ and the $\hat{P}_\varphi$ shown in Figs. 1(c) and (d) is smaller than the 4% of the absolute value of poloidal flux at the magnetic axis, $|\psi_{p,AXIS}|$, namely $|(\psi_{R_{TIP}} - \hat{P}_\varphi)/\psi_{p,AXIS}| < 4\%$. The results are shown in Fig. 12 with the solid curves, and the results by Condition 4 are

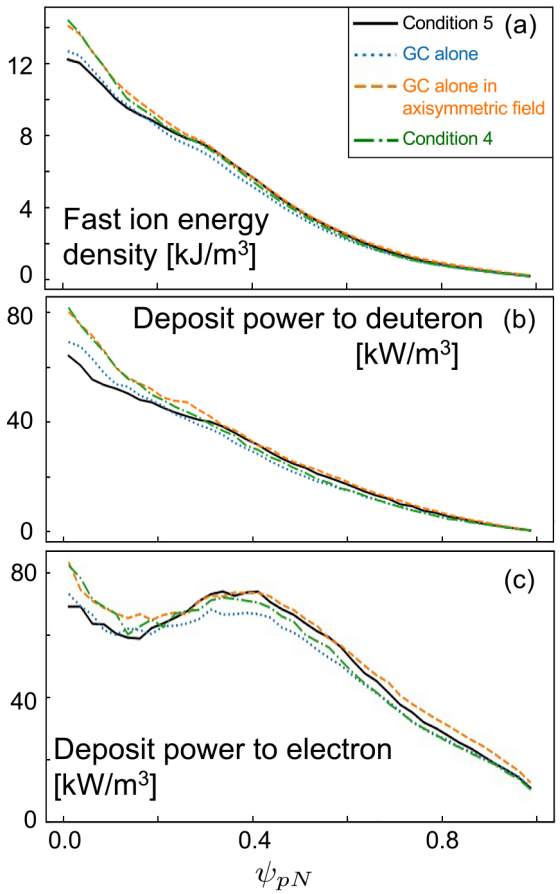

Fig. 12. Comparison of profiles of fast ion energy density (a), deposit power to bulk deuterons (b), and deposit power to bulk electrons (c). The results are depicted by black solid curves for Condition 5, green dashed-dot curves for Condition 4, blue dotted curves for the calculation by the GC method alone in the TF ripple and orange dashed curves for the calculation by the GC method alone in the axisymmetric field.

represented by the dashed-dot curves. A distribution in $\psi_{pN} < 0.4$ got close to the results by the GC method alone (the dotted curves).

As can be seen in Fig. 8(b), the ripple is less than 0.2% at $\psi_{pN} < 0.4$, but there is a ripple well region. In the region, the transport due to a trapped and detrapped mechanism in a local mirror or due to the ripple well is also possible, resulting in the change in the profile in $\psi_{pN} < 0.4$. Therefore, what was set to $\psi_{pN,TIP} > 0.4$ under Condition 3 was changed to $\psi_{pN,TIP} > 0.0$ (Condition 6). The results are shown by the solid curves in Fig. 13. The dashed-dotted curves are for Condition 5. At $0.2 < \psi_{pN} < 0.4$, the Condition 6 got close to the results by the GC method alone.

It is considered that the dominant ripple transport mechanism is included in Condition 6. Next, for a comparison, we carried out the calculation in which all banana particles are followed by the GC method in addition to Condition 5 where the GC method is used for particles near the boundary between banana and passing orbits (Condition 7). The results are shown by the solid curves in Fig. 14. The dashed-dotted curves are for Condition 6. Although there is a slight improvement, it is almost identical to Condition 6. We confirmed that Condition 6 almost takes into account the effect of the TF ripple on banana particles. Figure 15 shows a comparison of current drive and momentum drive in these cases. These show good agreements.

From the result for Condition 7, it appears that the remaining differences with the GC method alone are due to passing particles. Therefore, even for passing particles, when the bounce time is longer than $2 \times 10^{-4} \times \tau_s$ as in Condition 4 for banana particles alone, the GC method was used (Condition 8). The results are shown by the solid curves in Fig. 16. In this figure, the case of Condition 3 is shown by the dashed line, and the case of Condition 7 by the dashed-dotted curves. The Condition 8 got close to the results by the GC method alone.

At the end, we compare the total energy transfer ratio, total loss amount ratio, contribution ratio of thermalized test particles to the input power, and the calculation time in Table 2. When comparing the total amount, the difference from the GC method alone is a few % under Condition 3, and the calculation time is reduced to ~ 1/20. In the case for Condition 7 (Fig. 14), the distribution also shows a good agreement. In the case, although the calculation time is somewhat longer, it

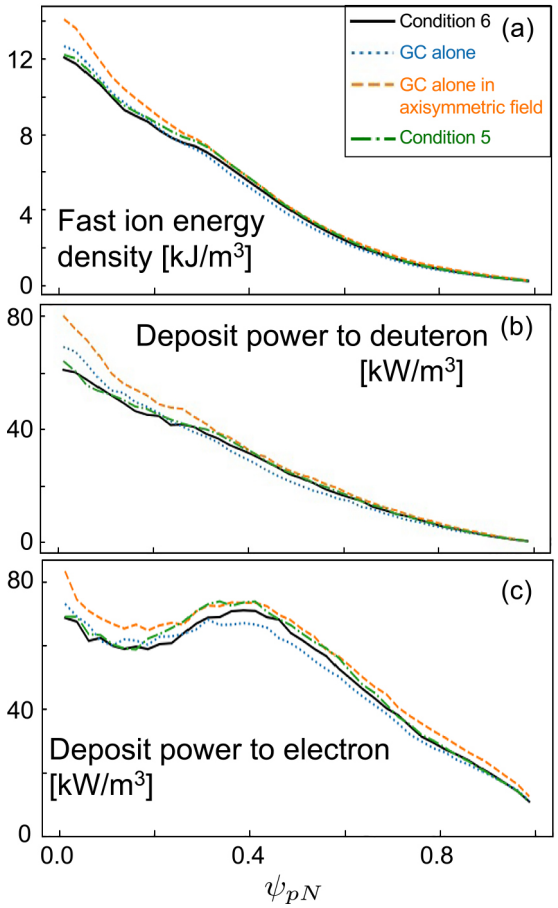

Fig. 13. Comparison of profiles of fast ion energy density (a), deposit power to bulk deuterons (b), and deposit power to bulk electrons (c). The results are depicted by black solid curves for Condition 6, green dashed-dot curves for Condition 5, blue dotted curves for the calculation by the GC method alone in the TF ripple and orange dashed curves for the calculation by the GC method alone in the axisymmetric field.

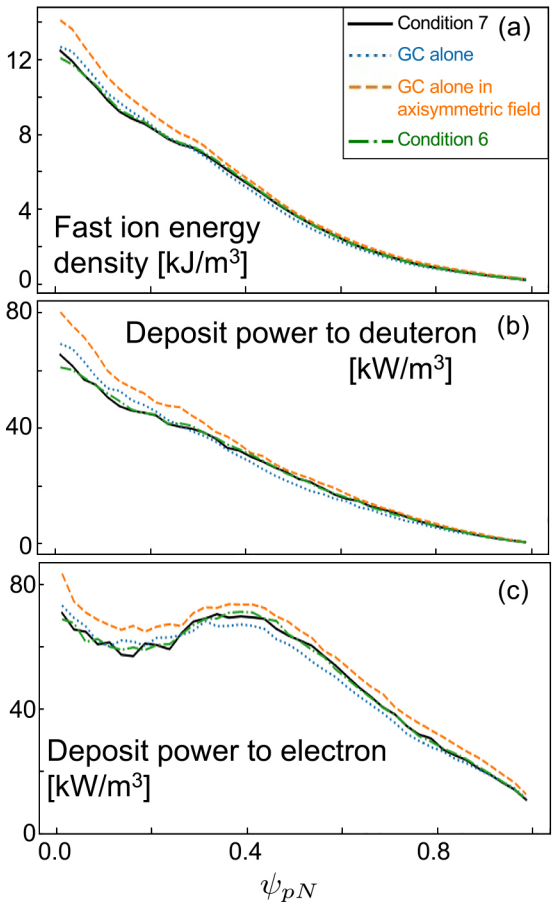

Fig. 14. Comparison of profiles of fast ion energy density (a), deposit power to bulk deuterons (b), and deposit power to bulk electrons (c). The results are depicted by black solid curves for Condition 7, green dashed-dot curves for Condition 6, blue dotted curves for the calculation by the GC method alone in the TF ripple and orange dashed curves for the calculation by the GC method alone in the axisymmetric field.

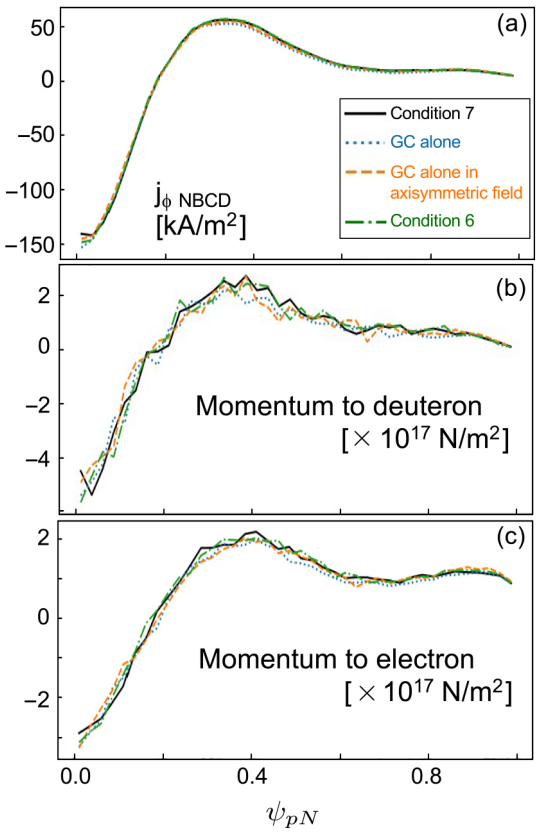

Fig. 15. Comparison of profiles of driven-toroidal-current density (a), momentum to bulk deuterons (b), and momentum to bulk electrons (c). The line-types are the same with those in Fig. 14.

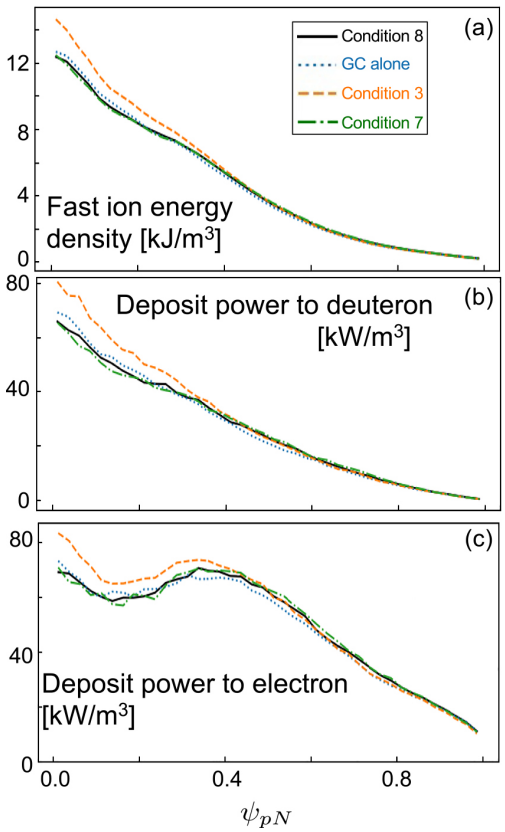

Fig. 16. Comparison of profiles of fast ion energy density (a), deposit power to bulk deuterons (b), and deposit power to bulk electrons (c). The results are depicted by solid curves for Condition 8, dashed-dot curves for Condition 7, dashed curves for Condition 3, and dotted curves for the calculation by the GC method alone.

Table 2. Total energy transfer ratio, total loss amount ratio, contribution ratio of thermalized test particles to the input power, and calculation time.

	GC alone (Dotted curves)	Condition 3 (Solid curve in Fig. 9): $R_{TIP} > R_{AXIS}$, $\psi_{pN,\,TIP} > 0.4$	Condition 4 (Dashed-dot curve in Fig. 9): Cond. 3 + $\tau_B > 10^{-4} \times \tau_s$ for banana	Condition 5 (Solid curve in Fig. 12): Cond. 4 + $\left\lvert \frac{\psi_{R_{TIP}} - \hat{P}_\varphi}{\psi_{p,\,AXIS}} \right\rvert < 4\%$	Condition 6 (Solid curve in Fig. 13): Cond. 5 + $\psi_{pN,\,TIP} > 0.0$	Condition 7 (Solid curve in Fig. 14): Banana + $\left\lvert \frac{\psi_{R_{TIP}} - \hat{P}_\varphi}{\psi_{p,\,AXIS}} \right\rvert < 4\%$	Condition 8 (Solid curve in Fig. 16): Cond. 7 + $\tau_B > 10^{-4} \times \tau_s$ for passing
Energy to Electron	50.0%	52.6%	51.9%	52.8%	51.4%	51.3%	51.0%
Energy to Ion	23.4%	25.9%	25.0%	24.2%	23.8%	23.7%	23.7%
Energy to Impurity	7.0%	7.3%	7.2%	7.0%	6.9%	6.8%	7.1%
Loss	18.5%	12.6%	14.5%	14.6%	16.7%	16.8%	17.1%
Contribution of thermalized test particles	1.1%	1.6%	1.5%	1.4%	1.3%	1.3%	1.1%
Calculation time [minutes]	197.0	9.1	23.8	27.5	26.9	22.5	44.6

is about 1/10 of the time required for the GC method alone. In this particular case, the calculation time got from 197 to 22 minutes. We achieved the reduction of the computing time or resource.

We may select a condition for purpose since the wall load is good agreement even for Condition 3 and the difference in global quantities are also small even for Condition 3, compared with the GC method alone.

6. Summary

We developed the BT orbit-following Monte-Carlo code to calculate a fast ion transport in the previous work as an extension of the OFMC code in QST [14]. However, the BT method has limitations in its realistic application. In order to reduce the limitation, we have developed a hybrid code with the BT method and the GC method. In the hybrid code, we can switch the methods depending on conditions. With using

this hybrid code, we have reduced the difference of fast ion energy density in the central region which was observed in the previous work. We have been able to adopt a realistic first wall as a loss boundary instead of a plasma surface or a separatrix too. From the result, we have been reminded that the finite orbit effect is important.

We have also applied this hybrid approach to handle the fast ion transport in a TF ripple. We set several conditions which can relate to the transport due to the TF ripple. The hybrid calculation well reproduced the profiles of several quantities by the calculation by the GC method alone while reducing the calculation time. Though we expected diffusion of banana tips (Condition 3) and the consideration of the ripple well would be sufficient for the conditions to treat the TF ripple, we have realized the contribution of passing particles is also important. As a future work, we would like to investigate an effective mechanism by which passing particles contribute to the transport by the TF ripple and to construct a reasonable condition for the mechanism for a hybrid approach.

As another future plan, we would like to handle a magnetic perturbation, considering a resonant condition. We know a resonant condition is important for transport. The resonant condition can be evaluated by using orbit helicity [16] (note that the orbit helicity is referred to as orbit pitch in Ref. 16). By switching the orbit-following methods with depending on the orbit helicity, we would like to improve the performance when handling the TF ripple. We also would like to handle an ELM-control perturbation [12, 13].

Acknowledgements

This work is partially supported by the Grant-in-Aid for Specially Promoted Research (No. 21H04973). This research was conducted using the Supermicro ARS-111GL-DNHR-LCC and FUJITSU Server PRIMERGY CX2550 M7 (Miyabi) at Joint Center for Advanced High Performance Computing (JCAHPC). We also would like to dedicate this paper to the memory of Dr. M. Azumi.

[1] N. Hayashi and JT-60 Team, Phys. Plasmas **17**, 056112 (2010).
[2] A. Fukuyama *et al.*, Proc. 20th IAEA FEC (Villamoura, Portugal, 2004) IAEA-CSP-25/CD/TH/P2-3.
[3] S. Mochinaga *et al.*, Nucl. Fusion **64**, 066002 (2024).
[4] K. Tani *et al.*, J. Phys. Soc. Jpn. **50**, 1726 (1981).
[5] K. Tobita *et al.*, Nucl. Fusion **35**, 1585 (1995).
[6] K. Shinohara *et al.*, Nucl. Fusion **47**, 997 (2007).
[7] K. Shinohara *et al.*, Nucl. Fusion **43**, 586 (2003).
[8] G.J. Kramer *et al.*, Nucl. Fusion **53**, 123018 (2013).
[9] JT-60SA Research Plan, https://www.qst.go.jp/uploaded/attachment/6690.pdf.
[10] K. Shinohara *et al.*, Fusion Eng. Des. **84**, 24 (2009).
[11] K. Shinohara *et al.*, Nucl. Fusion **51**, 063028 (2011).
[12] K. Tani *et al.*, Nucl. Fusion **52**, 013012 (2012).
[13] K. Shinohara *et al.*, Nucl. Fusion **52**, 094008 (2012).
[14] K. Shinohara *et al.*, Plasma Fusion Res. **20**, 1403017 (2025).
[15] B.A. Trubnikov, Rev. Plasma Phys. **1**, 105 (1965).
[16] K. Shinohara *et al.*, Nucl. Fusion **60**, 096032 (2020).